Dynamic Magnetic Properties of $Ca_3Co_2O_6$, TP 4 Report

Samuel WYLER
Supervisor: Ivica ZIVKOVIC
December 24, 2020

CONTENTS

I. INTRODUCTION

The structure of $Ca_3Co_2O_6$ was first described at the end of the last century.[1] The $Ca_3Co_2O_6$ crystals are interesting because of their special structure. They can be described by the quasi-one-dimensional Ising model, and the triangular arrangement of the spins makes it impossible to simultaneously minimise the energy at each bond.[2, 3] This leads to magnetic frustration. Low temperature measurements of the underlying magnetisation properties were done just after the first experimental evidence of the structure. While magnetisation is a linear function of the external field at $50\,\mathrm{K}$, it was found that for lower temperatures a sort of plateau emerges.[4] But the clear appearance of this $1/3M_s$ magnetisation plateau at $10\,\mathrm{K}$ is only one of the fascinating properties of $Ca_3Co_2O_6$[5]: by going beneath $10\,\mathrm{K}$ additional metamagnetic transitions appear.[6, 7] Moyoshi and Motoya et. al. focused then on the regions close to zero field.

What is less clear is the behaviour of $Ca_3Co_2O_6$ in non zero field at temperatures of $2\,\mathrm{K}$. Especially the dependent on time of the magnetic moment raises question. In fact, previous papers have only rarely mentioned the experimental procedure regarding waiting times, relaxing times, etc. At $2\,\mathrm{K}$ $Ca_3Co_2O_6$ becomes slow adapting to a change in field. This is where additional difficulties arise. This work provides an overview of the magnetic nature of $Ca_3Co_2O_6$ just below 3.5 Tesla at $2\,\mathrm{K}$. This field is not chosen by chance; at $10\,\mathrm{K}$ $Ca_3Co_2O_6$ shows a clear transition at $3.5\,\mathrm{T}$ where one spin per triangle flips. With this in mind, magnetic moment and susceptibility measurements on a timescale up to approximately 70 hours were made. Where possible these measurements are compared to previous in-house measurements on $Ca_3Co_2O_6$.[5] This was especially done for some prior susceptibility scans from 30 to $2\,\mathrm{K}$.

A more technical point of this work was to obtain a general understanding of the real limits of the Quantum Design MPMS3 machine in use. The MPMS3 is a recent investment. Issues corresponding to the different measuring modes shall be discussed along with the physics.

No immediate application but a general gain in knowledge emerges from this work. In the end, each piece of information leads towards a better understanding of basic processes in solids. Especially when it comes to the magnetic properties of solids, far-reaching fundamental knowledge seems to be

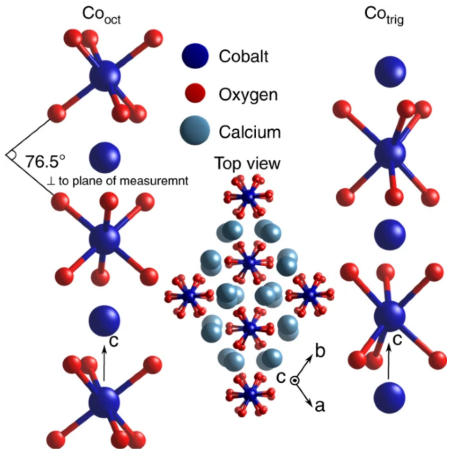

Fig. II.1: *Structure of $Ca_3Co_2O_6$. The two in the structure alternating types of Co environments with O ligands are shown and specified with Co_{oct} and Co_{trig}. The alternating Co environments form chains. The top view on the ab plane shows the triangular structure of $Ca_3Co_2O_6$. Graphic provided by Leedahl, Sundermann, Amorese,* et al.*[8]*

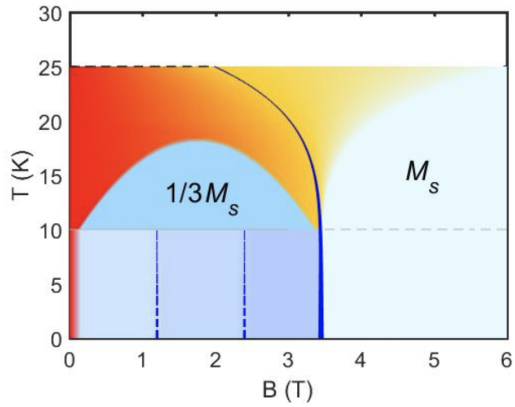

Fig. II.2: *Temperature - magnetic field phase diagram of $Ca_3Co_2O_6$, proposed by Hegde, Levatic, Magrez,* et al.*[5]*

indispensable in order to really understand groundbreaking discoveries and developments such as high-temperature superconductors.

II. Literature Review

The recently published paper on the magnetic dynamics across the in-field transition in $Ca_3Co_2O_6$ (CCO) [5] will be the leading paper for this work. In $Ca_3Co_2O_6$, magnetisation plateaus in low temperature regions - especially at 10 K - are nicely visible.[5] Its structure can be well described by the one dimensional Ising Model, which makes the theoretical understanding easier. The magnetic lattice in $Ca_3Co_2O_6$ is arranged in triangular form in the *ab* plane.[5] Figure II.1 present the structure of $Ca_3Co_2O_6$ visually. The two types of one dimensional Co chains along the *c* axes are represented, as well as the projected view on the *ab* plane. Each side of this triangle represents a spin which can point either upwards or downwards. With this explanatory approach of the magnetic structure of $Ca_3Co_2O_6$, four magnetisation plateaus can be satisfyingly described. Two of them actually correspond to the saturation magnetisation; ($\uparrow\uparrow\uparrow$) and ($\downarrow\downarrow\downarrow$).

Both ferromagnetic and anti-ferromagnetic interactions are found in $Ca_3Co_2O_6$. The first are the intra-chain interactions with an interaction energy of $J_1 \approx 24$ K,[9] the latter are the inter-chain interactions. The triangular patterns themselves are aligned on a quasi-one-dimensional chain. Since these chains are shifted by $\pm c/3$ in the compound, the weaker interaction force between different chains (inter-chain) become important.[5] In our framework, we will focus on measurements of non-zero fields. As already mentioned, we will see a strong dependence on temperature and magnetic field in our measurements, as these two different interactions are assumed to play against each other. This phenomena is not new and has been seen before.[6, 7] Nevertheless, the focus of these previous papers lay on the zero field magnetic moment behaviour, but ramping down from different field strengths (5 - 1.8 T) and different temperatures (1.9-5.75 K).[7] We will see similarly strong dependence on external field and temperature in non-zero field measurements.

The magnetic properties of $Ca_3Co_2O_6$ do not adapt immediately to new external conditions. There is another parameter: time. This time dependency of magnetic properties is only rarely explored in $Ca_3Co_2O_6$. From the experimental point of view, the parameters of interests have to set in a manner that they lead to time dependent behaviour on machine measurable time scales. We will see that these timescales can be changed by magnitudes by varying environmental temperature or the imposed magnetic field.

In literature, saturation magnetisation is given as $M_s = 5.2\mu_B$, where μ_B is the Bohr magneton. This seem to be in good agreement with neutron scattering.[6]

We consider a singular triangular pattern with spins originally pointing in the same direction ($\uparrow\uparrow\uparrow$). Three spins, symmetric under the symmetry group D_3, do change their direction completely in three transitions ($\downarrow\downarrow\downarrow$). The three transitions lead to four plateaus, which are $M_s, \frac{M_s}{3}, \frac{-M_s}{3}, -M_s$. These transitions are commonly named $\mathcal{J}_-, \mathcal{J}_0, \mathcal{J}_+$.[5] The leading paper [5] then describes the $\mathcal{J}_0$ transition, which is the one going through $M = 0$ as following. Not all triangular patterns change their states at once, but the change starts in some small droplets and then grow bigger up to the moment the new level is achieved.[5] This process include time dependence. We will focus on the behaviour close to the saturation magnetisation which means $\mathcal{J}_-$ and $\mathcal{J}_+$ are of interest.

See Fig.II.2 for the temperature - magnetic field phase diagram of $Ca_3Co_2O_6$ as it is understand today.[5] The clearly defined boundary of the phase of magnetic saturation M_s starts to fade above 10 K. The regime where the $1/3M_s$ plateaus appear has a superior temperature limit as a function of the external magnetic field. Note that it was clearly verified that at low temperatures ($\leq$ 10 K) metamagnetic transitions appear when measuring magnetic moment versus applied

field. These metamagnetic states appear to be in relation with spin density waves which are not further considered in this context. But Kamiya and Batista supposes that the low dynamics below 10 K are a direct consequence of the multiple SDW micro phases discovered below 25 K.[6, 10] Furthermore the ramping down of the magnetic moment below 10 K does not match with the ramping up; a hysteresis is observe.

The leading paper was primarily focusing on the region $T \geq 10$ K. There the influence of time in the measurements can be neglected. If there were dynamics the system anyway adapt faster than we can measure to the new environment. This report will focus of on the region beneath 10 K.

In order to not go beyond the scope of this work, in this report I will focus on a phenomenological rather than theoretical description.

III. Theory

A deepened understanding of the magnetic behaviour of $Ca_3Co_2O_6$ is difficult in temperature ranges below 10 K. The newly introduced time component complicates measurements. First, one must determine on which timescale the physics actually occurs. When measuring in DC-mode an order of magnitude of seconds is the lower technical limit. The upper limit is given by our patience, to put it in a casual way. Parameters such as the external magnetic field and temperature will be proven as central in the accelerating or slowing down of physical relaxation processes. However, while for humans the linear scale is most natural, in physics this is often no longer true. Logarithmic timescales provide often a more precious insight in the physical world than a linear it does. Therefore, it is natural to switch our timescale as soon as possible into a logarithmic one. The results will underpin this.

Still, the fine tuning of the $Ca_3Co_2O_6$ system remains complicated. Taking for example the external magnetic field B[1]: we suppose that the $Ca_3Co_2O_6$ crystal would respond immediately to the application of an external magnetic field. If this were the case, we would measure in this case a simple magnetic moment versus Field plot. The curve on this plot would have plateaus, transition regions and perhaps even less understood metamagnetic transition regions. Either way we would be able to assign to each set of external conditions a response, a magnetic moment of the crystal.

Interestingly, in very low temperature regions of 2-10 K, $Ca_3Co_2O_6$ does not behave as simply as this. Time comes into play which means, when we change the environment $Ca_3Co_2O_6$ does not respond immediately but adapts in a nonlinear manner in time to the new circumstance. This effect is truly time dependent, and becomes stronger with lower temperatures. Focusing on $T = 2$ K, higher temperatures will only be mentioned in passing. On the other hand, many different fields will be considered. But exactly here an unavoidable difficulty arises. For example, if we ramp the exterior field from saturation down to 2 T, then the "targeted" magnetic moment which will be achieved after infinite time is *approximately* predetermined. It is different when we ramp down to 2.5 T. But not only are these "targeted" moments different, but also the rate of achieving them! Consequently, the difficulty of description arises precisely in this duality. Being more exact these "targeted" moments are a characteristic of the equilibrated state which will be achieved (ignoring quantum fluctuations) after an infinity of time.

Furthermore, note that time is in all these measurements an additional and only barely controllable parameter. Outside of practical reasons the time in our laboratory can neither be accelerated nor slowed down. The time parameter is always present.

We will call the process of approaching the equilibrated state relaxing. It may be that the usage of relax is an abuse of the original meaning of this word. Still, it seems the best description of the given situation.

IV. Experiment Setup and Applied Techniques

It seems fundamental to describe the most important physical and technical functions of the measurement methods which are used in this project. Starting with the central physical aspect of our measurement, which brings the *QU* into *SQUID*[2].

A. Flux Quantization

An important ingredient is the quantization of the magnetic flux, which follows as a necessity from the study of Superconductors (SC).[3] We work with a device whose mode of operation is based on this quantization. The following is a theoretical derivation. Let us consider a SC ring. The current density travelling around this ring can be given by the 1^{st} Landau Gingsburg equation (LG):

$$\mathbf{j} = i\frac{e\hbar}{m}\left(\Psi^*\vec{\nabla}\Psi - \Psi\vec{\nabla}\Psi^*\right) - \frac{4e^2\mathbf{A}}{mc}\Psi^*\Psi \tag{1}$$

where m is the electron mass, e the elementary charge, $\mathbf{A}$ the vector potential, c the speed of light and Ψ the order parameter. By setting $\Psi = |\Psi|e^{i\phi}$ Eq.(1) is simplified to:

$$\mathbf{j} = \frac{2e\hbar}{m}|\Psi|^2\left(\vec{\nabla}\phi - \frac{2e}{\hbar c}\mathbf{A}\right) \tag{2}$$

where $|\Psi| = \Psi^*\Psi$, the modulus of the order parameter. But because of the Meissner effect, the magnetic field $\mathbf{B}$ beyond the penetration length λ is zero. From this follows that the curl of $\mathbf{B}$ is zero. Thanks to Maxwell's laws and the knowledge that there is no changing electric field, it can be concluded that the current density $\mathbf{j}$ is also zero. The bracket on the RHS of Eq.(2) has to be zero. By integrating the bracket term over the ring, which constitutes a closed circle, we obtain:

$$\frac{\hbar c}{2e}\oint \nabla\phi \cdot d\mathbf{l} = \oint \mathbf{A}\cdot d\mathbf{l} = \oint \boldsymbol{\nabla}\times\mathbf{A}\cdot d\mathbf{S} = \int \mathbf{B}\cdot d\mathbf{S} \tag{3}$$

[1] Note that for practical aspects the term *magnetic field* is used, we actually mean *Magnetic flux density* throughout the whole report.

[2] Standing for: Superconducting QUantum Interference Device

[3] The following is inspired by Mila.[3]

For the final equality, by applying Stokes Theorem the magnetic flux through a surface is identified. After integrating once around the circle, Ψ must remain in the same form, which is only possible if the phase changes by a multiple of 2π along the integration path. Thus, Eq.(3) is simplified,

$$\Phi = n\frac{\pi\hbar c}{e}, \qquad \Phi_0 = \frac{\pi\hbar c}{e} \tag{4}$$

where we have found that the magnetic flux is quantized in units of Φ_0. This Φ_0 is called the magnetic flux quantum and have a value of $2.068 \times 10^{-7}\,\mathrm{emu}$. However, this quantization is so small that without a SQUID device it is hardly measurable Note that this quantization is indispensable for the explanation of persistent currents in SC: a SC with induced current is always in a (heavily) exited state. The normal behaviour of such a system in the continuous world would be to fall back in the ground state (GS) fast.

B. Basis of SQUID Measurements

Now that we are aware that the magnetic flux is quantized through a superconducting ring, the next goal is to describe qualitatively the functional principle of DC SQUIDs (cf. Fig.IV.1). Superconducting Quantum Interface Devices consist of two so called Josephson junctions (JJ) in parallel. JJ are made out of a sandwich of two superconductors connected by a normal region (SNS). Bardeen–Cooper–Schrieffer theory (BCS) supposes that electrons appear in Cooper pairs in the superconducting parts. For a long time it was supposed that passing the normal region is only possible after breaking these pairs up, which costs an energy 2Δ. B. Josephson, a Welsh physicist, discovered as a graduate student that this is not the whole truth.[11] A junction current appears already long before a potential difference of $\frac{2\Delta}{e}$ for breaking of the Cooper Pairs is available. This is a tunnelling effect which allows current through a normal region without any voltage drop over the junction. This shall give us a first hint that with an appropriate machine one can achieve a new incredibly small lower limit for measurement sensitivity.

By taking Eq.(2) and setting $\mathbf{A} = 0$, we see that current in a SC is based on a non-uniform phase of the order parameter $\Psi = |\Psi|e^{i\phi}$. A current through the SNS junction is therefore possible as long as the phase is varying along it. In a SQUID the current is induced by a magnetic flux, but supposing the current is induced by a potential difference, this difference is never bigger than infinitesimal. An estimate of the critical current density $\mathbf{j_c}$ is found by modifying Eq.(1) and setting the phase difference to $\pi/2$, which maximises the sine which is found in an intermediate step. The gradient of the function which describes the phase in the normal region is assumed to be of the form $1/L$, where L denotes the width of the normal region. The critical current density up to which no potential difference appears across the junction is thus given by,

$$\mathbf{j_c} = \frac{2e\hbar}{m}|\Psi|^2\frac{1}{L} \tag{5}$$

The wider the normal region becomes, the lower the critical current that can flow through the normal range becomes.

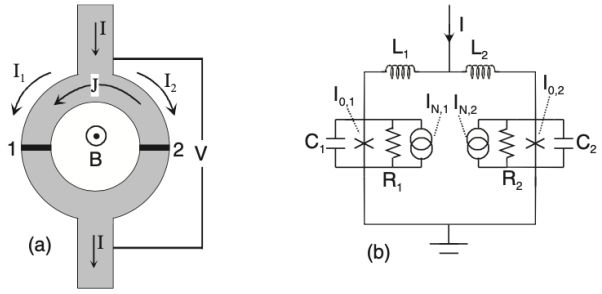

Fig. IV.1: *a.) Schematic drawing of a SQUID with two Josephson Junctions. b.) Electronic circuit of the describing RCSJ model.[12]*

In conclusion, a SQUID is a ring reacting to a magnetic flux passing through it. A good description a real SQUID is given by the "Electronic circuit of resistively and capacitively shunted Josephson junctions" (RCSJ) model (cf. Fig.IV.1). This flux induces a current J in the SQUID ring, in order to compensate the non-integer part of the flux. Additionally, to this induced current J we can let a bias current I_b[4] flow through the SQUID. Note that we denoted in Eq.(5) with $\mathbf{j_c}$ the critical current density in Josephson junction but with I_c we denote the critical current over the whole SQUID. This general critical current is the key to DC SQUID measurements. As long as $I_b < I_c$, no potential difference is measured over the SQUID. This changes as soon as $I_b > I_c$, where the ohmic regime starts.

Consider now the current in the two SNS junctions: $I_{SNS,\pm} = \frac{I_b}{2} \pm J$. But as soon as $I_{SNS,-} > I_c$ one junction wants to change into the ohmic voltage regime because the current density is now higher than allowed for tunnelling (Eq.(5)). Remember the other junction has at this moment still a null resistivity so the current immediately tries to pass through this junction. As consequence, a complicated interfering of the two junction starts. The result of this interfering is that the overall critical current I_c is periodically modulated by the magnetic flux passing through the SQUID. The periodicity is Φ_0. In conclusion, one takes advantage of the SC's inability to cope with non-integer magnetic fluxes.

To measure the magnetic flux, either an electronic which repeatedly searches for $I_b = I_c$ is used, or one works constantly in a regime slightly above the I_c. In the latter case, one uses the fact that in this regime the flux is in places approximately proportional to the voltage measured over the SQUID.

The explanations of DC-SQUID dynamics fill books. Let us focus on the central results - first the final expression for the critical current:

$$I_c = 2I_0\left|\cos\left(\pi\frac{\Phi_a}{\Phi_0}\right)\right| \tag{6}$$

where Φ_a denotes the flux through the SQUID, Φ_0 the previously found magnetic flux quantum and I_0 the averaged critical current.[12]

[4] In the Figure IV.1, denoted by I.

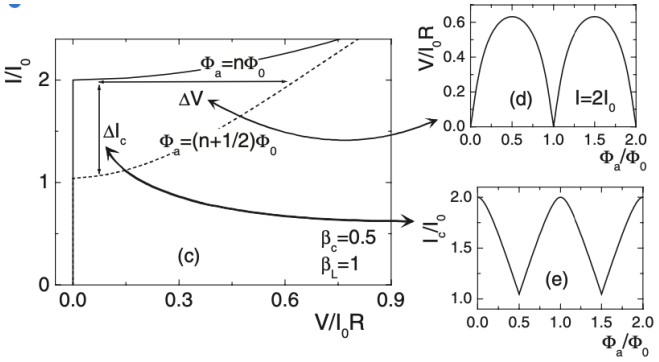

Fig. IV.2: *LHS: Characteristic diagram of the normalised current against the normalised potential for the two extreme situations in which a whole or half multiple of Φ_0 flow through the SQUID ring. RHS: Voltage and current in function of the flux. All numerically calculated.[12]*

With further derivation the current-voltage characteristics for $I_b > I_c$ are given by

$$V = \frac{R}{2}\sqrt{I^2 - I_c^2}, \tag{7}$$

which makes clear why the voltage oscillates with a period of one magnetic flux quantum (Φ_0). The right side of figure IV.2 shows the normalised voltage(current) across(in) the SQUID as a function of magnetic flux.

All these calculations are simplified[5]; for example we set $T = 0$ K to avoid thermal fluctuations.

C. Thermal and $1/f$ Noise

Let us first take a look at thermal noise, but notice that this kind of noise is less important in low temperature applications. Thermal noise is present in all electrical circuits. If the noise is independent of frequency we call it *white* noise. We are primarily interested in ensuring that the noise current does not exceed the critical current across the SQUID. The thermal noise is proportional to the temperature: $I_{th} = \frac{2\pi}{\Phi_0} k_B T$.([12], p.39) We get a lower limit for the minimal critical current, since for a clear signal $I_{th} < I_c$. By recalling Eq.(5), this imposes a limit on the width of the normal region when fabricating junctions. In general, for high temperature applications the junctions have to become smaller.

The so called $1/f$ noise, or Pink Noise, should be a more important factor for the work at hand. This is a frequency dependent noise where the spectral density has the following form: $S(f) \propto \frac{1}{f^\alpha}$ ($\alpha > 0$). Pink noise is a vast subject that appears in diffusion processes, biological processes, earthquake analysis and also electronics - SQUID electronics.[14, 15] In a SQUID, we deal with two sources of pink noise; fluctuations in Josephson junctions and flux lines trapped in the body of the SQUID.[12] The former occurs by faulty tunnelling through the normal region due to defects in the same. As a result, the tunnel barrier starts to fluctuate and so does the critical current density $\mathbf{j_c}$. We call these imperfections traps. Without doubt the noise power spectrum is strongly dependent on the junction quality. Nevertheless, the general form, assuming $D(\tilde{E})$ is a broad energy distribution, is

$$S(f,T) \propto \frac{k_B T}{f} D(\tilde{E}) \tag{8}$$

where $D(\tilde{E})$ is the distribution of the relevant trapping energies.[12, 16]

In conclusion, we note that the extent of noise and its treatment in SQUID electronics is far beyond the scope of this paper. Nevertheless, the proportionality of temperature and the existence of $1/f$ will be needed later.

D. Electronics and Readout

As we have seen above, a DC SQUID works as a flux to voltage translator. The voltage profile is periodic with a period of one flux quantum Φ_0 (cf. Eq.(6) and (7)). Concentrating on the flux change during measurement we see that this can be best measured where the slope of $V(\Phi_a)$ is maximised. Note that Fig.IV.2 presents a simplified situation, in reality the current flattens out more close to the minima. We call these two points (one left, one right of the maximum) *working points* and they are best because a change in Φ_a leads to the biggest change in voltage and the transferring is to a good approximation linear. We can write:[17]

$$\delta V = V_\Phi \delta\Phi_a, \qquad V_\Phi = \frac{\partial V}{\partial \Phi_a} \tag{9}$$

Note that once $\delta\Phi_a$ becomes too big we quit the linear transferring region. The adjustment of the working point is done by varying the bias current I_b. In order to enlarge the dynamic range a *flux locked loop* (FLL) is applied which feeds back the deviation from the working point by means of a magnetic back coupling with the SQUID.[12, 18] An additional coil with negligible impedance in the target frequency range is installed for this reason.

Concretely by means of an amplifier the deviation from the working point voltage V_b (which is predefined) is amplified and then integrated. The amplification gain (for example controlled with a feedback resistivity element) defines the range adaption of the SQUID. Supposing a flux *range* of $100\Phi_0$ which is exceeding the linear part of Fig.IV.2 by far, a magnetic feedback flux proportional to the deviation of the V_b with gain 1000 can reduce the actual felt magnetic flux range of the SQUID by factor 1000 to $0.1\Phi_0$. Even without applying sophisticated error calculations (which are necessary because of the assumption of linearity in this new range) the baseline importance of this feedback loop becomes clear. The SQUID machine at hand will use 1, 10, 100 and 1000 as re-ranging factors.

Finally, an analogue-digital-converter (ADC) is used before the data can be processed by computers. Here, problems can arise because the measurement range is larger than the

[5]Further on parameters as $\beta_c = \frac{2\pi}{\Phi_0} I_0 R^2 C$ which is the Stewart-McCumber parameter and $\beta_L = \frac{2LI_0}{\Phi_0}$ the screening parameter are restricted; $\beta_L << 1$ (negligible inductance), $\beta_C << 1$ (negligible capacity).[13]

converter can handle. To eliminate this issue a counting and reset mechanisms come into play, eg. when the Flux Locked Loop loses track. All these mechanisms allows the machine to combine exact small range measurements without loosing the view on possible much larger flux range. The SQUID itself is periodically reset by a rapid heating above the critical temperature of the SC. This is done to omit residual circuit currents which persist for a long time, as we have seen in section IV-A.

It is clear that SQUID electronics goes much further than basic principles discussed here. A major point is the handling of noise; lock-in detection, for example, allows the extraction the signal of known frequency from strong background noise.[19]

E. Specific Experimental Details

For more information about the crystal growth of $Ca_3Co_2O_6$ consider [5], since samples of this production cycle were used. For all measurements the *Magnetic Property Measurements System 3* (MPMS3) of QUANTUM DESIGN is used. MPMS3 works using a SQUID and knows three different measurement modes including DC-, VSM- and an additional AC-mode. The temperature range in the evacuated chamber is 400 to $1.8\,\mathrm{K}$. The applied magnetic field is able to reach $7\,\mathrm{T}$, the maximum ramping speed is given by $700\,\mathrm{Oe/sec}$. The charging resolution is small with $0.33\,\mathrm{Oe}$, but without quenching the remanent field is typically around $5\,\mathrm{Oe}$.[20] Measurement scans are added up in so-called sequences. The output data is analysed by means of MATLAB first, and later with PYTHON. This is mainly to improve PYTHON skills. As a first step, I focused on understanding and applying the basics of data analysis and representations in PYTHON. However, the number of scans reached quickly a number of 100 and therefore a basic database with a convenient class for the scans is used to keep scans in order.

1) DC Measurements: The DC scans are all taken by similar sequences and setups. Prior to commencing the scans, the external field is ramped up to $7\,\mathrm{T}$ with the intention to get rid of possible hysteresis, the saturation moment is measured, and the magnets ramped down to the target field where the measurement starts. The start of the ramping to the target field defines $t_0 = 0$, so that the results become comparable. Remember the saturation was found and verified to be $M_s = 5.2\mu_B$, where μ_B denotes the Bohr Magneton.[5, 6]. We found a slightly lower value of $M_s = 4.9\mu_B$. Then the magnetic moment of the $Ca_3Co_2O_6$ sample is measured continuously - either in DC or VSM mode. The measurement duration was of the order of hours. The time resolution is especially in DC-mode limited to f_m $=0.2\,\mathrm{Hz}$, where f_m denotes the sampling rate. An issue is the ramping speed limitation of $700\,\mathrm{Oe/s}$ which prevents a proper analysis of the first minutes. Note that the sample starts relaxing once $3.5\,\mathrm{T}$ (for $T \leq 10$ K) is reached although the ramping down process can still take up to 2 minutes. Two samples are in use for the measurements; one carefully fixed in a plastic straw, a second on a quartz sample holder. The samples weights are $1.3\,\mathrm{mg}$ and $3.5\,\mathrm{mg}$ respectively. The special reason for the usage of a quartz sample holder is explained below, but note that in the end also the majority of DC-mode results presented in this report is obtained by using the $3.5\,\mathrm{mg}$ sample.

For simplicity in DC Mode the *fixed* magnetic moment is used throughout.[6] The difference to the *free* magnetic moment is in general marginal and a re-calibration of the sample position is done once the sample was cooled down to $30\,\mathrm{K}$.

2) VSM Measurements: VSM-mode scans are performed in the same way as those in DC-mode. The key difference in the sequences is the lack of a saturation measurement at $7\,\mathrm{T}$. The only sample that comes into question for VSM-mode measurements is the one on the quartz sample holder with a weight of $3.5\,\mathrm{mg}$. Straw sample holders are simply not rigid enough to sustain the rapid sample movement in VSM-mode. To avoid a long and technical explanation of VSM measurements, here is a brief overview of the working principle. VSM stands for *Vibrating Sample Measurements* and was first extensively described in a paper in 1959 by Foner. As the name is saying the sample is vibrating perpendicular to classical detection coils. The magnetic moment of the sample, according to Maxwell's laws, induces a voltage in this coil. The magnetic moment is proportional to the induced voltage. Once calibrated, the sensitivity of the first machines in the year 1959 was already in the order of $10^{-5} - 10^{-6}$ emu.[21] Later when SQUIDs became available, the pick-up coils mentioned above were - in simplified terms - just replaced by a SQUID. This means that SQUID-based machines can also benefit from rapid VSM measurements.

3) AC Measurements: AC mode scans are subject to certain unexpected limitations, which are pointed out in the "Problems" section. The measuring frequencies are always chosen as non-integers to avoid coupling with the laboratory respectively auxiliary electronics due to insufficient shielding. For AC-mode scans, both the straw ($1.3\,\mathrm{mg}$ sample) and the quartz ($3.5\,\mathrm{mg}$ sample) sample holder are used. However, the results presented in this report are mainly obtained by using the $1.3\,\mathrm{mg}$ sample. Although wider test measurements were done, the scans presented here are all done with $1\,\mathrm{Oe}$ (Fig.V.1) and later $0.1\,\mathrm{Oe}$ (Fig.V.2) AC-driving amplitude. The ranging was set *sticky* instead of *always auto*, which is default and does not adapt the SQUID ranging for every single point. Results were not affected in tests. When one single point is measured in an AC-Mode scan this point actually is the average of a whole set of measurement.

A delicate question is how to define or limit the number of these sub-measurements for averaging. By predetermining a fixed dwell time in each configuration, the following issue emerges: while for high frequencies enough repetitions can be

[6]The manual describes: "The "Fixed Center" values denote the analysis result where the sample position is determined by the AutoTracking algorithm, the moment thus being the only free parameter for the fit to the raw data."[20]

done, this may not be the case at low frequencies. An example, at 991 Hz the order of 10'000 more repetitions are done in the same time interval as at 0.1 Hz. In the end, this problem was handled by a machine feature that allows a target cycle number and a target time. Depending on the frequencies, the value which leads to a longer averaging time is always taken. In the first two presented scans (cf. Fig.V.1), this method with $n_{cycles} = 12$ and $t_{point} = 6$ s is applied.
But remark that this can still be misleading because much more sub-measurements are done at higher frequencies. Finally, the most honest way is to simply predefine a number of repetition cycles; 10000 in our case for the third sequences where the focus is on 991 Hz (cf. Fig.V.2). For both variants the total measured time per configuration is multiplied by time since the 5-point technique have to be applied (cf. section VI). Without doubt, these parameters have been played around with in order to find an optimum between machine occupation time and reliability. The final chosen values are probably not the best choices, but they are largely acceptable.

In order to offer a quantitative comparison with [5] as well as a qualitative one, the atomic mass of $Ca_3Co_2O_6$ was determined as (334.064 39 u)[22] to infer the number of moles and to normalise the susceptibility values.

For all graphs presented as a function of time, the relative time indicated on the axes starts counting when the magnets begin to ramp to their target field.

V. Results

A. Susceptibility of $Ca_3Co_2O_6$ at low Temperatures

The recently published paper by Hegde, Levatic, Magrez, *et al.* presents susceptibility measurements of $Ca_3Co_2O_6$ in two different magnetic field environments. These measurements were done on a commercial Quantum Design PPMS. We try to replicate those results on the recently installed Quantum Design MPMS3. Figure V.1 provides the susceptibility χ' in zero field (middle of $\mathcal{J}_0$ transition) and 1.85 T ($1/3M_s$ plateau) field over an identical temperature range. Comparing to [5] we provide a few lower frequencies which results in χ' not falling back to zero when cooling to 2 K in zero field. In $B = 1.85$ T, noise overshadows especially low frequencies[7]. It is suspected that this is $1/f$ noise suppressing problem. The lower frequency limit for acceptable noise treatment is assumed to be in the order of magnitude of 100 Hz. Hegde, Levatic, Magrez, *et al.* does not provide lower frequencies either. However, the significant frequencies (in colour) do qualitatively reproduce the recently found results.
In addition, we find that the AC sensitivity is reduced in the range 17-30 K somewhere below 80 Hz.

We omit the plot of errors in Fig.V.1 because the standard error in the zero field is on average three orders of magnitude smaller than the results;
$\sigma(\chi')$=0.004 emuOe^{-1}mol^{-1}. The trustworthy results at 1.85 T behave the same; $\sigma(\chi')$=0.003 emuOe^{-1}mol^{-1}. But below 20 Hz; $\sigma(\chi')$=0.03 emuOe^{-1}mol^{-1}, which becomes unacceptable. Note in particular that this is the average, there are outliners with errors orders of magnitude higher.

[7] In the lower graph of Fig.V.1 the measurements at 30 K are intentionally not shown because of the faulty machine behaviour. Compare section VI.

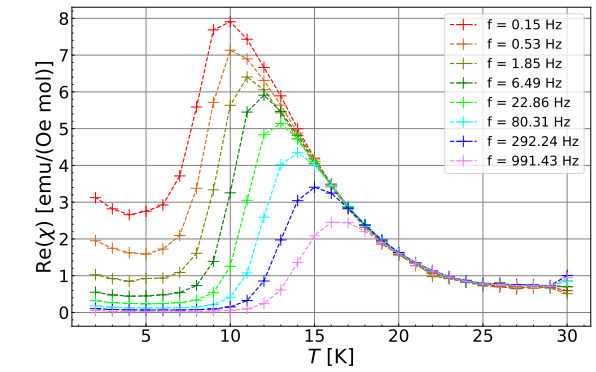

(a) *In* $B = 0$ *T*

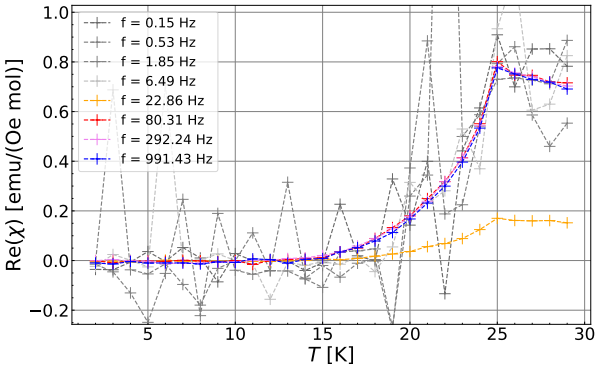

(b) *In* $B = 1.85$ *T*

Fig. V.1: *Temperature dependence of AC Susceptibility for a logarithmic distributed frequency set.*

With the reasoning of having lowest Pink Noise, further susceptibility considerations are done at f =991 Hz. Again, a temperature range between 2 and 30 K is scanned, the fields are set according to the lower and upper edge of the $1/3M_s$ plateau. It can be seen from Figure V.2 that above approximately 20 K, $Ca_3Co_2O_6$ susceptibility is slightly higher in magnetic fields on the upper edge ($\geq$ 2.35 T) compared to the lower edge of the $1/3M_s$ plateau.

As we will see below the response of the magnetic moment and therefore the spins in this temperature range ($\geq$ 20 K)is fast enough, such that the time component can be ignored. The $Ca_3Co_2O_6$ response (adaption) speed to the environment can be assumed as immediate.

From a technical side below 15 K a few outliers appear. They can not be described by just assuming a high noise level, since noise is problematic in most of the cases, especially in high temperatures (cf.IV-C). It should be reduced in low temperature environments. It seems that there is still another at the moment unknown issue with the AC-module.

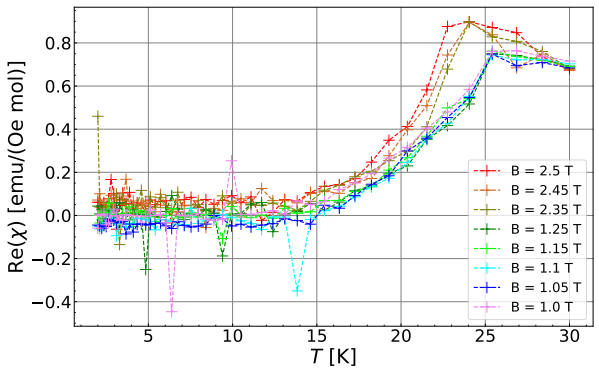

Fig. V.2: *Temperature dependency of AC Susceptibility in different fields both on the lower and upper edge of the* $1/3Ms$ *plateau. AC frequency equal to* 991 Hz.

B. Magnetic Moment at $T = 2$ K

1) Time, an important Factor in $Ca_3Co_2O_6$: Figure V.3 provides an overview of the importance of a good understanding of temporal effects in $Ca_3Co_2O_6$ at low temperatures. The y-shift across the different curves is produced by the $Ca_3Co_2O_6$ relaxing in time. Consequently, the "lowest" curve is measured in the slowest changing external magnetic field. Therefore, it is able to relax the most. This is a strong indicator of $Ca_3Co_2O_6$ not adapting immediately to the environment at low temperatures - here 2 K. The metamagnetic transitions which were already discussed in papers appear in Fig.V.3.[6, 7] The labels are positioned as proposed by Moyoshi and Motoya: $B'_{c1} = 0.1$ T, $B'_{c2} = 0.8$ T, $B'_{c3} = 1.2$ T and $B'_{c4} = 2.3$ T. They match to a good extend the previously found results which were elaborated at 1.9 K. The lower the ramping rate, the clearer the metamagnetic transitions appear. Nevertheless, these data must be interpreted with caution because of the changing relaxing-timescale due to the scanning along a magnetic field range.

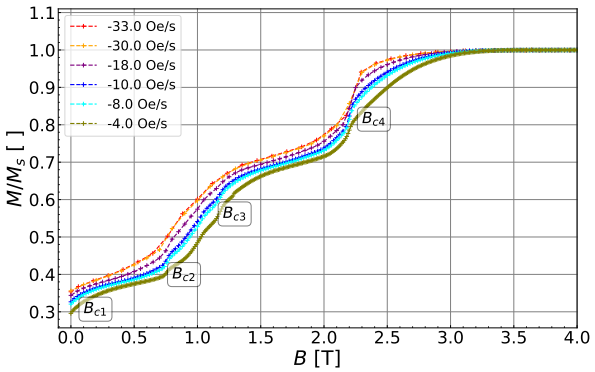

Fig. V.3: *Magnetic moment versus external field scan at* 2 K. *The labelling gives the average ramping rate of the external field. In reality the ramping is not constant but achieved by various waiting times in the field scan. Labelling of meta-magnetic transitions as done by Moyoshi and Motoya.[6]*

2) The Magnetic Moment as a Function of Time and Field: The previous sections introduced the dangers of a hasty interpretation of low temperature measurements. This section will investigate the dependence of time in a more structured manner. The results show a non-linear dependence of the relaxation process on the applied field.

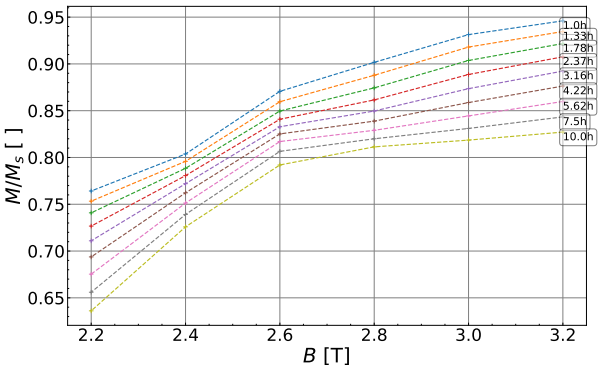

Fig. V.4: *Magnetic moment of $Ca_3Co_2O_6$ at various fields. Curves differ in the absolute time of relaxation which is lapsed. T = 2 K.*

Considerations on magnetic moment in $Ca_3Co_2O_6$ are made at 2 K primarily. Prior to a step-by-step analysis of the raw data, we present in Figure V.4 a significant outcome. The plot illustrates the way in which the magnetic moment of $Ca_3Co_2O_6$ relaxes in time as a function of the applied external field. The "glimpses" are logarithmically distributed over time. As mentioned in the reference article, the sample no longer have saturation magnetisation as soon as the value falls below 3.5 T.[5] Below 10 K and especially at 2 K this value is well defined. While beneath 2.6 T the curves become steeper, a flattening-out happens in the first 3 h, this could be due to the B'_{c4} metamagnetic transition.[6] Interestingly after letting $Ca_3Co_2O_6$ relax for a longer time (7.5 − 10 h) this is no longer true - the curves gain steepness. Anyway, this could also be due a faulty 2.2 T measurement.

Turning now towards the raw data - gathered as described in the experiment setup section. The logarithmic x-axes allows us to read out much more information that on a linear time scale. As shown in Figure V.5a the magnetic moment relaxes not perfect exponentially in time. The curves appear to be rescaled by changing the applied magnetic field, consider 3.2, 3, 2.8 T. Nevertheless our rescaling attempts were not satisfying. In this work at least 3 inflection points are identified during the relaxation process. In order to get their exact values the gradient must be calculated. The application of *Savitzky–Golay-* and *median* filters before and after calculating the gradient is indispensable[8]. In addition, the filter parameters must be varied along time axes, due to the logarithmic time scale.

Figure V.5b presents the correct derivatives for a plot with logarithmic x-axes. Inflection points are now given by curve extremes which are marked with a cross. The raw, unfiltered data is available in the annex (cf.Fig.A.2b). The

[8]Raw data can be found in the Annex A, Fig.A.2b

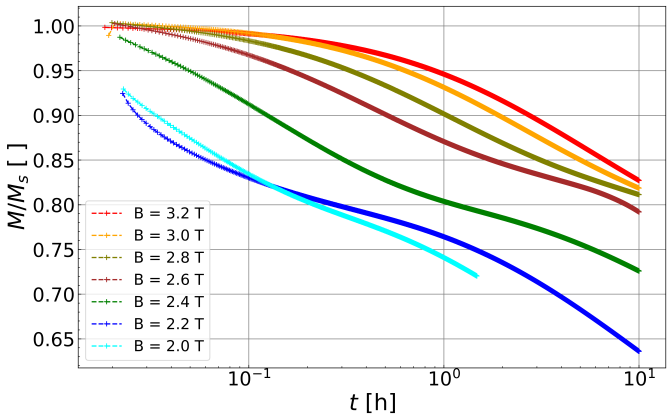

(a) *Magnetic moment as a function of time in different external fields. T = 2 K.*

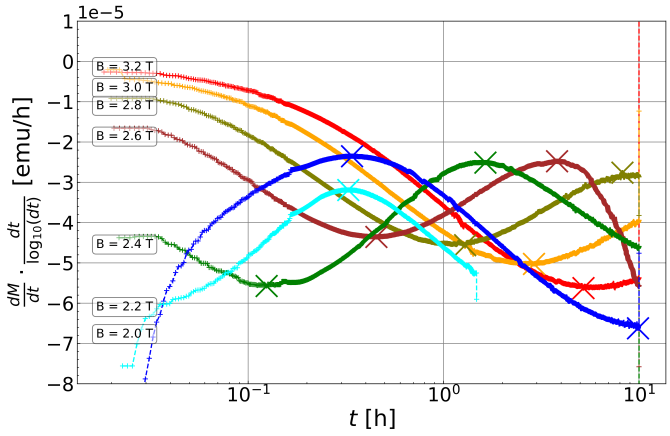

(b) *First time derivative of magnetic moment as a function of time. Derivative adapted to the logarithmic x-axes. Extremes marked with cross.*

curves are again shifted against each other according to the external field. The cyan coloured scan at 2 Tesla was stopped early. Also, the 2.6 Tesla scan suffered under an unwanted temperature raise in the last 5 hours up to 2.12 K (cf. Fig.A.2a in the annex). Although not optimal, no negative impact was found.

Consequently, Figure V.6 compares the magnetic moment at the occurrence of inflection points as a function of the external field. The bullet points describe the more trusted DC mode data, the crosses represent the VSM-mode data set. Interestingly, a pattern appears; especially the inflection points of 2nd order[9] decrease with the applied magnetic field B, no clear trend can be found for the 1st inflection points. In $B = 2$ T the 3rd inflection point would appear as well if the measurement had not been stopped before reaching a time of 10 h. All magnetic moments are normalized with the same averaged saturation value. Note that especially in the VSM-mode a significant offset in the magnetic moment was discovered. This is why these results should be considered with caution. Arguing in this way, we dispense with linear fitting.

We turn now to a final analysis of the inflection of

[9]Note that the word *order* should not be misunderstood; the field is ramped down at initial time and the first inflection of the magnetic moment in time is called 1st order, and so on.

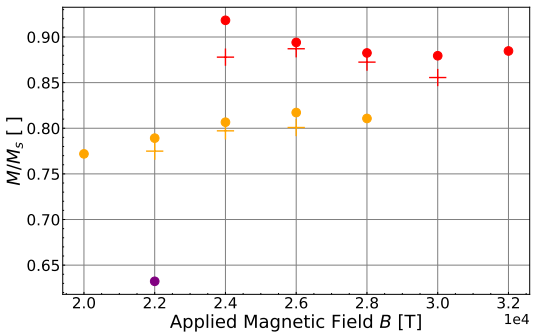

Fig. V.6: *Magnetic moment at deflection point as a function of the exterior field (environment).*
×: 1^{st} *infl. / VSM mode;* ●: 1^{st} *infl. / DC mode;*
×: 2^{nd} *infl. / VSM mode;* ●: 2^{nd} *infl. / DC mode;*
●: 3^{rd} *infl. / DC mode.*

magnetic moment in time. To each inflection not only a magnetic moment but also a relative time (after ramping to the target field) can be assigned. The results obtained are compared in Table V.6. All available data at 2 K are presented. What is noticeable is the decrease in time as a function of applied field until the inflections occur. It also turns out that the 2^{nd} inflection times differs from the 1^{st} order inflection times by the same order of magnitude - a factor of approximately 10 for all fields. A closer look reveals that the fraction $\frac{t_{i,2}}{t_{i,1}}$ is in general growing with the decreasing external magnetic field.

Field B [T]	Mode	$t_{i,1}$ [h]	$t_{i,2}$ [h]	$t_{i,3}$ [h]	$\frac{t_{i,1}}{t_{i,2}}$ []
3.2	DC	5.21	-	-	-
3.0	DC	2.9	-	-	-
3.0	VSM	3.9	-	-	-
2.8	DC	1.29	8.24	-	6.39
2.8	VSM	1.12	-	-	-
2.6	DC	0.45	3.81	-	8.47
2.6	DC long	0.39	3.95	-	10.13
2.6	VSM	0.34	-	-	-
2.4	DC	0.12	1.64	-	13.67
2.4	VSM	0.16	1.53	12.75	
2.2	DC	-	0.34	9.9	-
2.2	VSM	-	0.36	-	-

TABLE I: *Conclusive table with relative time after ramping of magnets when inflection of 1^{st}, 2^{nd} or 3^{rd} order appears.*

C. Critical Exponent Techniques - An Approach

Another approach to the description of the relation between external magnetic field (temperature) and the relaxation timescale uses the theory of critical exponents. It became clear that the relaxation cannot be described by a simple exponential curve; this is why the idea of using power laws for a local linearisation came into play. Although this approach looked promising at the beginning, no generalisation was possible, neither for the field varied scans nor the temperature varied scans.

In general, the idea is to describe the behaviour of the magnetic moment as a function of time by a critical exponent. As presented in Figure V.7 with a power law

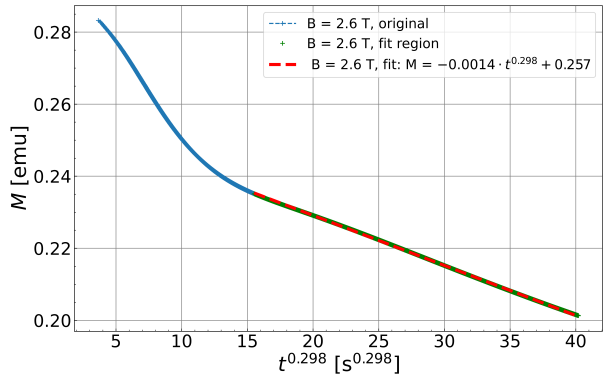

Fig. V.7: *The Magnetic moment as a function of time, represented on a power law x-axes. Measurement taken at 2 K over 68 h. The standard deviation the fitted exponent is acceptable* 1.79×10^{-04}.

imposed on the x-axes, a local linearisation is achieved. The theory of critical exponents was originally developed as theory to describe phenomenologically all sorts of phase transitions. One found that different physical systems possess the same critical exponent despite having different transition points. Could it be, that although the magnetic moment relaxation in different fields or at different temperatures look qualitatively different, they all have the same critical exponent for a certain region of relaxation? The magnetic moment would then have the following form:

$$M \sim (-t)^{\mu}, \tag{10}$$

where t is the time and μ the critical exponent. The results were not satisfying, either because of the impossibility to identify the region to linearize or because such an exponent simply does not exist. Note that Fig.V.7 represents a $68\,\mathrm{h}$ measurement while all other data is restricted to $10\,\mathrm{h}$.

For clarification, the "transition points" in Fig.V.7 are compared to the position of inflection points of the $68\,\mathrm{h}$ measurement at $2.6\,\mathrm{T}$. The inflection points are positioned at $t_{i,1} \approx 0.39$ h and $t_{i,2} \approx 3.953$ h while the regime change discussed happens at ≈ 14.3 h. No correlation can be found between these two approaches.

Also, fitting with a linear combination of exponential functions, as done in previous works [6] around the $0\,\mathrm{T}$ was not satisfying. Not even local fitting with simple exponential functions was satisfying.

D. Timescale Change with Temperature

Turning for completion toward the dependency on temperature, the external magnetic field is each time ramped down to $3.4\,\mathrm{T}$. Figure V.8 presents the raw relaxation curves. Generally, the higher the temperature, the faster the relaxation. For $T \geq 3$ K the MPMS3 ramping rate is again too low to catch the first minutes. Note the massive change of timescale on which the relaxation happens. According to [5] at 10 K $Ca_3Co_2O_6$ is ruled by the $\mathcal{J}_+$ transition occurring at $3.5\,\mathrm{T}$, the magnetic moment then is $M = 0.334 \cdot M_s$. Beneath this, and in extremes at $1.9\,\mathrm{K}$[6] metamagnetic states dominate the $Ca_3Co_2O_6$ behaviour. What happens in between is unclear. But relaxation is nowhere purely exponential. While at $2\,\mathrm{K}$ the relaxation is only accelerated after $10\,\mathrm{h}$, at $9\,\mathrm{K}$ it tends towards zero after $10\,\mathrm{h}$.

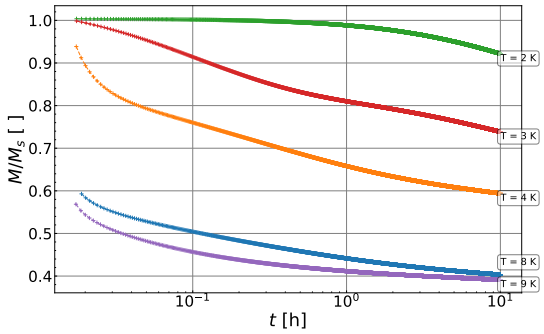

Fig. V.8: *The Magnetic moment as a function of time relaxing at different temperatures in* $3.4\,\mathrm{T}$ *external field.*

VI. Machine Issues

It is not unusual for newly installed machines to have certain peculiarities. Following an overview:

- AC mode: Susceptibility Phase Offset
- AC mode: Issues with 1- and 3-point technique
- AC mode: Faulty first measurement
- AC mode: High Pink noise
- VSM mode: General offset
- DC mode: General offset
- General: Necessary recalibration of sample offset after cooling down from ambient temperature.

And some issues further discussed.

Susceptibility Phase Offset

The machine on hand is equipped with an AC-mode option. This additional module was recently replaced because of faulty behaviour. It turned out that in AC-mode results include a phase offset of up to π. The susceptibility results presented above are in this sense all phase corrected by a value of π, here 5-point measuring techniques were used. It is not clear in what type of pattern, if any, this phase offset occurs. Further tests have been executed by supervisor I. Zivkovic, this time with the 1-point technique. Using old results, we determined the phase (offset) in regions where we would expect a phase equal to zero. This offset was then applied to the entire scan. A short PYTHON function was written for this purpose. The offset is far from being constant, and no pattern is made out. Consider for a visualisation the annex A.

Issues with 1- and 3-Point Measurement Method in AC-Mode.

In AC-mode only scans with 5-point measuring applied gave trustworthy results. The machine itself logged errors

when using the 1- or 3-point measuring option. *SQUID RAILED* was for example one of the errors showed. There is no explanation in the manuals beyond a mention of a possible occurrence.

VSM Offset

The saturation magnetisation M_s at 7 T was in VSM-mode never determined for $Ca_3Co_2O_6$. Nevertheless, at 2 K magnetisation of $Ca_3Co_2O_6$ should be equal for 4 T, 3.8 T and 3.6 T - the sample's magnetisation should be saturated. Note that because of emerging hysteresis beneath 10 K the stand-by field is always 7 T. But $\bar{M}_s(B = 4T) = 0.2889$ emu, $\bar{M}_s(B = 3.8T) = 0.2828$ emu, $\bar{M}_s(B = 3.6T) = 0.2805$. $\bar{M}_s(B = 3.6T)$ is almost 3% lower than $\bar{M}_s(B = 4T)$ emu which is not acceptable. Quantum Design specifies the VSM mode sensitivity of the MPMS3 as $\leq 8 \times 10^{-8}$ emu in fields larger than 0.25 T.[20] Figure A.1a in the Appendix illustrates this. Manipulation errors seem unlikely, but are not taken into account due to the small number of VSM scans.

DC Offset

In DC-mode the saturation magnetisation at 7 T was determined prior to each scan. Surprisingly, we were confronted with unexpected fluctuation in these measurements. These fluctuations do not follow a pattern, a technical machine issue seems likely. We then checked correlation with other log data such as temperature, sample offset position or SQUID range, without success. We found strong correlation with the provided measurement error, and weak correlation with the DC SQUID drift. We refrain from calculating the exact correlation because the data set is weak but still provides a good visual overview. Figure VI.1 provides the visualisation. It can be concluded that the machine is "aware" of the general offset. A SQUID drift could be the reason, but more tests should be done.

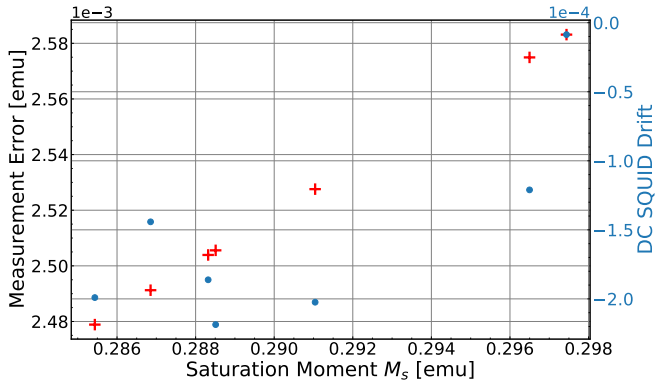

Fig. VI.1: *Magnetic moment of $Ca_3Co_2O_6$ at saturation versus the temperature at measurement. External magnetic field set to 7 T.*

Faulty First Measurement in AC-Mode

Another issue which usually occurred is the following: the first AC measurement in a scan is executed with the wrong parameters and gives hardly interpretative results back. First of all, the "AC-frequency" is often just set to 1 Hz as well as "AC-Cycles" to 1, in conclusion the AC Averaging Time is faulty. On the output side no standard error is provided. It is not clear whether the results are trustworthy but measured with wrong parameters or the results itself are faulty.

Compare this with Fig. V.1 where the first point is measured at 30 K. However, these faults do not appear consistently all the time; take Fig.V.2 as an example. **The driving amplitudes are different in this case; 0.1 Oe is fault free.**

$1/f$ Noise in Low Frequency AC-Susceptibility Measurements

Most impressively shown in FigV.1, the source of this issue is difficult to investigate. It is not fully understood if this noise is of (faulty) technical origin or in the range of the physical limitation of the MPMS3 System. In general sources of noise are numerous.[23] In the present case the frequency dependence lets us focus on the above described SQUID $1/f$ noise issues. Nevertheless, electromagnetic interferences with mechanical devices (cryogenic or motors) which couples with the AC Drive frequencies are not completely excluded. Mechanical vibration on the other hand is mostly unable to resonate beneath 1 Hz. Poor shielding from power grid or domestic electronics working frequencies ($\approx$ 50 Hz) seems unlikely to be the case. However, it must also be said that these are consistently avoided.

VII. Discussion of Physical Findings

A. *Susceptibility at Low Temperatures*

When comparing the measurements at 0 T and 1.85 T, the high vulnerability to noise of the latter at low frequencies is particularly striking. The reason for this seems to be a technical one since for the 991, 292 and 80 Hz scans the standard error is one order of magnitude smaller than that measured in zero field. For 23 Hz the standard error is already two orders of magnitude. Nevertheless, this inadequacy is partly disappointing, as the sensitivity of the MPMS3 is specified with $\leq 5 \cdot 10^{-8}$ emu.

Remember in 1.85 T and around 10 K $Ca_3Co_2O_6$ is on the $1/3M_s$ plateau as stated in the leading paper, which stands out due to great stability of the ($\uparrow\uparrow\downarrow$) configuration.[5] This could be the reason for the lower response compared to the zero field scans. The lines of the scans below $\approx$23 Hz were faded out with the argument of low reliability. Nevertheless, it may be that these low frequencies would also follow the stable response of the 991, 292 and 80 Hz scans. However, this would call into question the validity of the lowering in susceptibility of the 23 Hz scan.

In zero field, the decrease of high frequency susceptibility below 10 K is not astonishing. In particular

below 10 K $Ca_3Co_2O_6$ responds slowly. This is underlined by the emergence of hysteresis. The reaction to a fast oscillating field becomes marginal, since the system is too inert for excitations. Analogies in the field of classical mechanics are numerous. Only frequencies close to the field in the range of 0.1-10 Hz allow a reaction. A first indication of the implication of time dependencies is therefore already found in the AC-mode measurements.

B. *Magnetic Moment at $T = 2$ K*

Different approaches were discussed to phenomenologically explain the relaxation behaviour of $Ca_3Co_2O_6$ at $T = 2$ K. The approach of using a universal critical exponent as known from phase transitions was not effective. Surprisingly the analysis of the inflection points is promising. We learnt that a logarithmic timescale in $Ca_3Co_2O_6$ gives insights which are not possible on a linear timescale. This in turn makes it difficult to measure the whole relaxation process.

The inflection points show a pattern which should allow a linear fitting. Nevertheless, more scans should have been done for evidence. In total 3 inflection points were identified. It remains open if there is even a 4^{th}, and if in all fields from 2 to 3.2 T all these inflection points appear. This furthermore evokes the question to what target magnetic moment $Ca_3Co_2O_6$ would relax after infinite time. Previous papers stated hysteresis behaviour beneath 10 K but were often vague about the waiting times in their measurements. [5–7] When talking about times: the time analysis of inflection appearance again supports the quasi-exponential behaviour of $Ca_3Co_2O_6$ during relaxation. Unfortunately no fitting curve was found.

It could be revealing to compare the $Ca_3Co_2O_6$ behaviour to spin glasses. Spin glasses have a memory of what happened in the past which goes much further than what we know from hysteresis behaviour. It was found that when spin glasses are cooled down, this process is memorised in the spin structure. Furthermore there exists an ageing temperature which lets the sample forget.[24] Concerning $Ca_3Co_2O_6$ there is a lot of knowledge missing as to if and in which sense there is a memory behaviour a low temperatures. Could it be that $Ca_3Co_2O_6$ does not imprint the temperature history, but the external field history? In a broad sense, this is exactly what happens through the hysteresis. But the results give one hope that not only the field but also the history of dwell times could play a decisive role. This would evoke the question of the existence of ageing field. A lower noise level in AC-mode would be indispensable to measure a broad bandwidth or rather low frequencies around 2 K. But these susceptibility measurements could give precious insights. In the study of spin glasses this is a key technique.[24, 25] If there is interest to investigate further in this memory direction, first of all a parameter which enables work on an appropriate timescale should be found. Then one could start to not only measure relaxation but seek memory effects by dwelling at different fields for different times. This would show if there are actual memory effects or "only" complicated relaxation behaviour.

In addition to spin glasses, the so called microstates, studied by Kamiya and Batista, seem to be in connection with the slow relaxation of $Ca_3Co_2O_6$ at low temperatures. This paper simulated $Ca_3Co_2O_6$ numerically by mean of a frustrated quantum Ising model. They were able to reproduce the above mentioned spin density waves which arises from the crystallisation of domain walls, leading to a large number of competing metastable states.[10]

VIII. Conclusion

Notwithstanding the limitations in AC mode, the preliminary susceptibility measurements are satisfying. They reproduce the results of the leading paper to a good extend. However, the full potential of the machine is especially in AC-mode not yet realised. In addition we showed that the growth in response to lower frequencies does not stop at 21 Hz. We also show a difference in susceptibility at 991 Hz between field strengths corresponding to the upper and lower edges of the $1/3M_s$ plateau.

Turning to DC-mode measurements at T =2 K, a wide and not yet satisfactorily described topic opens up. There is abundant room for further investigation of the rescaling of the relaxation properties by varying the external field. The inflection point analysis on a logarithmic time scale seems to be the most promising characterisation of these processes. A description with critical exponent was unsatisfactory. We showed that there are at least 3 such inflection points which occur at similar magnetic moments for all field strengths from 2 T to 3.2 T. A higher data density would help to find more exact dependencies of one on the other. In terms of time, we find an indication that the proportion of the occurrence times of the first and second inflection points could increase as the external magnetic field decreases. Typical values are 6.4 in 2.8 T to 13.7 in 2.4 T. However, one can justifiably criticise the low data density.

A suggestion for further work would be to increase temperature marginally by 0.5 - 1 K in order to accelerate the relaxation of $Ca_3Co_2O_6$ and safe machine occupancy time. Further studies on the influence of temperature could be added. In a later step a deeper comparison with spin glasses is suggested as well as intense comparison with computer simulations of the frustrated quantum Ising model. This would make the time parameter in particular easier to control. Simulation is not reality, but it could predict behaviour that requires multiple days of measurement.

I have to admit that especially the theoretical understanding, which is mandatory to understand the physical processes in their full depth, is often limiting. Often the question arises whether similarities between existing findings and our results are over-interpreted. Diving into this matter has proven to be

extremely challenging from both a technical and a physical point of view. One personal insight leads to another. The insight into the technical possibilities as well as all the difficulties and developments behind them are fascinating. A good choice of parameters of time and applied magnetic field is indispensable to to even measure what is expected.

References

[1] H. jellvag, E. Gulbrandsen, S. Aasland, A. Olsen, and B. C. Hauback, "Crystal structure and possible charge ordering in one-dimensional $Ca_3CO_3O_3$," *J. Solid State Chem*, pp. 190–194, 1996.

[2] A. Maignan, C. Michel, A. Masset, C. Martin, and B. Raveau, "Single crystal study of the one dimensional ca," *The European Physical Journal B*, vol. 15, p. 657, 4 Jun. 2000, ISSN: 14346028. DOI: 10.1007/s100510051169. [Online]. Available: http://link.springer.de/link/service/journals/10051/bibs/0015004/00150657.htm.

[3] F. Mila, "Solid state physis iii," EPFL, 2020.

[4] S. Aasland, H. Fjellvåg, and B. Hauback, "Magnetic properties of the one-dimensional $Ca_3Co_2O_6$," *Solid State Communications*, vol. 101, pp. 187–192, 3 Jan. 1997, 4lead, ISSN: 00381098. DOI: 10.1016/S0038-1098(96)00531-5.

[5] N. Hegde, I. Levatic, A. Magrez, H. M. Ronnow, and I. Zivkovic, "Peculiar magnetic dynamics across the in-field transition in $Ca_3Co_2O_6$," *Physical Review B*, vol. 102, 10 Sep. 2020. DOI: 10.1103/PhysRevB.102.104418. [Online]. Available: http://arxiv.org/abs/2009.08201%20http://dx.doi.org/10.1103/PhysRevB.102.104418.

[6] T. Moyoshi and K. Motoya, "Incommensurate magnetic structure and its long-time variation in a geometrically frustrated magnet $Ca_3Co_2O_6$," *Journal of the Physical Society of Japan*, vol. 80, 3 Mar. 2011, ISSN: 00319015. DOI: 10.1143/JPSJ.80.034701. [Online]. Available: https://journals.jps.jp/doi/abs/10.1143/JPSJ.80.034701.

[7] K. Motoya, T. Kihara, H. Nojiri, Y. Uwatoko, M. Matsuda, and T. Hong, "Time and magnetic field variations of magnetic structure in the triangular lattice magnet $Ca_3Co_2O_6$," *Journal of the Physical Society of Japan*, vol. 87, 11 Oct. 2018, ISSN: 13474073. DOI: 10.7566/JPSJ.87.114703. [Online]. Available: https://doi.org/10.7566/JPSJ.87.114703.

[8] B. Leedahl, M. Sundermann, A. Amorese, A. Severing, H. Gretarsson, L. Zhang, A. C. Komarek, A. Maignan, M. W. Haverkort, and L. H. Tjeng, "Origin of ising magnetism in $Ca_3Co_2O_6$ unveiled by orbital imaging," *Nature Communications*, vol. 10, p. 5447, 1 Dec. 2019, ISSN: 2041-1723. DOI: 10.1038/s41467-019-13273-4. [Online]. Available: http://www.nature.com/articles/s41467-019-13273-4.

[9] G. Allodi, P. Santini, S. Carretta, S. Agrestini, C. Mazzoli, A. Bombardi, M. R. Lees, and R. D. Renzi, "Exchange interactions in $Ca_3Co_2O_6$ probed locally by nmr," *Physical Review B - Condensed Matter and Materials Physics*, vol. 89, p. 104 401, 10 Mar. 2014, ISSN: 1550235X. DOI: 10.1103/PhysRevB.89.104401. [Online]. Available: https://journals.aps.org/prb/abstract/10.1103/PhysRevB.89.104401.

[10] Y. Kamiya and C. D. Batista, "Formation of magnetic microphases in ca 3co 2o 6," *Physical Review Letters*, vol. 109, p. 067 204, 6 Aug. 2012, ISSN: 00319007. DOI: 10.1103/PhysRevLett.109.067204. [Online]. Available: https://journals.aps.org/prl/abstract/10.1103/PhysRevLett.109.067204.

[11] *Brian d. josephson — british physicist — britannica*. [Online]. Available: https://www.britannica.com/biography/Brian-Josephson.

[12] B. Chesca, R. Kleiner, and D. Koelle, *Squid theory*, May 2005. DOI: 10.1002/3527603646.ch2.

[13] W. C. Stewart, "Current-voltage characteristics of josephson junctions," *Applied Physics Letters*, vol. 12, pp. 277–280, 8 1968, ISSN: 00036951. DOI: 10.1063/1.1651991. [Online]. Available: https://ui.adsabs.harvard.edu/abs/1968ApPhL..12..277S/abstract.

[14] E. Milotti, "1/f noise: A pedagogical review," Apr. 2002. [Online]. Available: http://arxiv.org/abs/physics/0204033.

[15] P. Szendro, G. Vincze, and A. Szasz, "Pink-noise behaviour of biosystems," *European Biophysics Journal*, vol. 30, pp. 227–231, 3 2001, ISSN: 01757571. DOI: 10.1007/s002490100143. [Online]. Available: https://api.semanticscholar.org/CorpusID:24505215%20https://www.tandfonline.com/doi/abs/10.1081/JBC-100104145.

[16] M. B. Weissman, "1f noise and other slow, nonexponential kinetics in condensed matter," *Reviews of Modern Physics*, vol. 60, pp. 537–571, 2 Apr. 1988, ISSN: 00346861. DOI: 10.1103/RevModPhys.60.537. [Online]. Available: https://journals.aps.org/rmp/abstract/10.1103/RevModPhys.60.537.

[17] D. Drung and M. Mück, *Squid electronics*, May 2005. DOI: 10.1002/3527603646.ch4.

[18] J. M. Kim, Y. H. Lee, H. Kwon, K. W. Kim, and K. K. Yu, "Flux-locked loop circuit, flux-locked loop method, and squid measuring apparatus," Apr. 2012.

[19] *Principles of lock-in detection — zurich instruments*. [Online]. Available: https://www.zhinst.com/ch/en/resources/principles-of-lock-in-detection.

[20] "Product description magnetic property measurement system." [Online]. Available: https://www.qdusa.com/products/mpms3.html.

[21] S. Foner, "Versatile and sensitive vibrating-sample magnetometer," *Review of Scientific Instruments*, vol. 30, pp. 548–557, 7 1959, ISSN: 00346748. DOI: 10.1063/1.1716679.

[22] D. R. Lide, W. M. ". Mickey, ". Haynes, G. Baysinger, H. V. Kehiaian, L. I. Berger, K. Kuchitsu, M. Frenkel, D. L. Roth, and R. N. Goldberg, "Crc handbook of chemistry and physics 90 th edition," 2010.

[23] C. P. Foley, M. N. Keene, H. J. T. Brake, and J. Vrba, *Squid system issues*, May 2005. DOI: 10.1002/3527603646.ch7.

[24] K. Jonason, P. Nordblad, E. Vincent, J. Hammann, and J.-P. Bouchaud, "Memory interference effects in spin glasses," 2000, pp. 99–105.

[25] J. Hammann, V. Dupuis, J. P. Bouchaud, E. Vincent, A. Ito, and H. A. Katori, "Aging, rejuvenation, and memory effects in ising and heisenberg spin glasses," *Physical Review B - Condensed Matter and Materials Physics*, vol. 64, 17 2001, ISSN: 1550235X. DOI: 10.1103/PhysRevB.64.174204.

APPENDIX

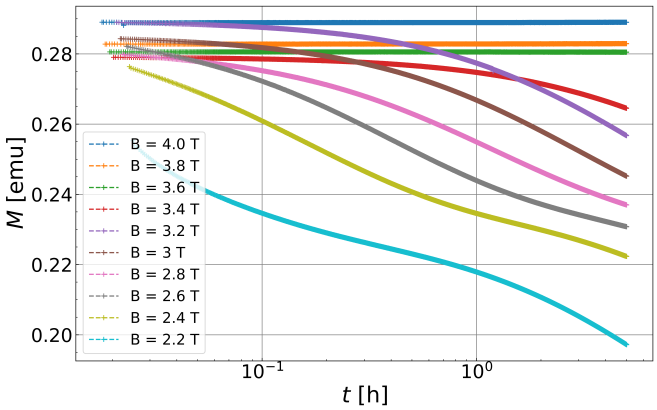

(a) *Magnetic moment measured with VSM-mode at 2 K in different external magnetic fields.*

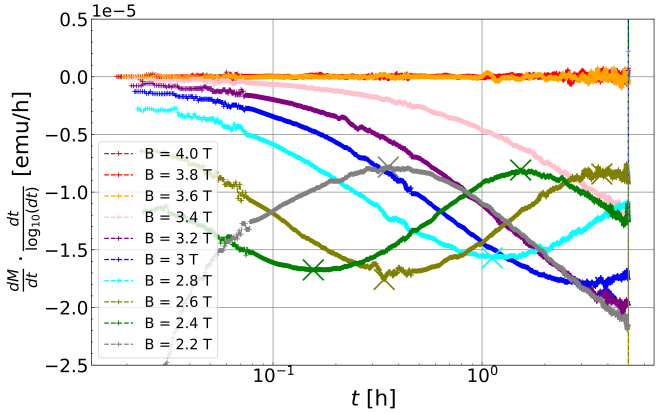

(b) *First time derivative of magnetic moment as a function of time. Derivative adapted to the logarithmic x-axes. Extremes marked with cross.*

Fig. A.1: *VSM-mode measurements*

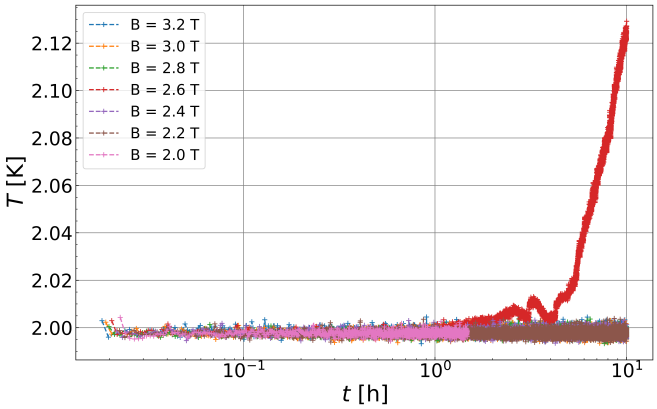

(a) *Unintended temperature rise of the 2.6 Tesla DC-mode scan (10 h.) Although not optimal no negative impact on the results has been found.*

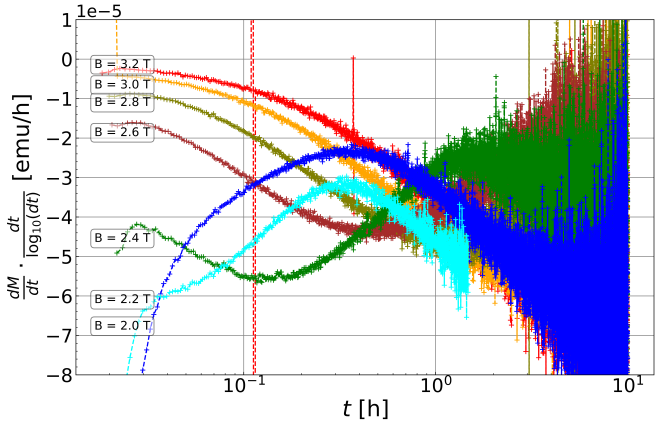

(b) *First time derivative of magnetic moment as a function of time. Derivative adapted to the logarithmic x-axes. Extremas marked with crosses.* ***Original - no filtering applied!***

Fig. A.2: *General additional plots of the DC-mode scans $Ca_3Co_2O_6$.*

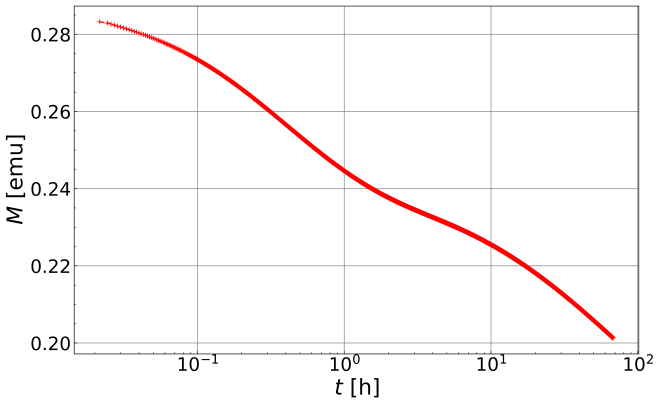

(a) *Magnetic moment as a function of time.*

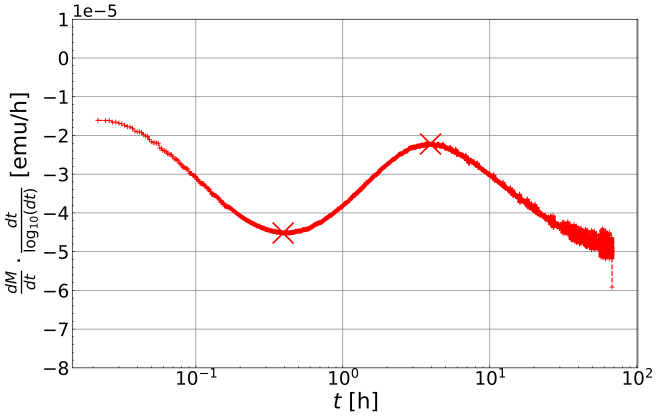

(b) *First time derivative of magnetic moment as a function of time. Derivative adapted to the logarithmic x-axes. Extremas marked with cross.*

Fig. A.3: *DC-mode 68 h measurement at 2 K and in 2.6 T external magnetic field.*

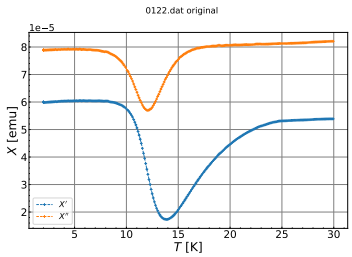

(a) *Original Temperature Scan for Susceptibility*

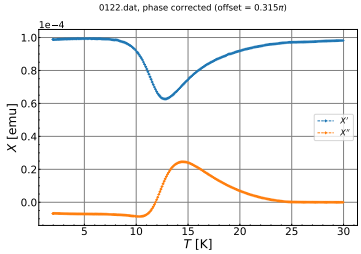

(b) *Phase Offset corrected Temperature Scan for Susceptibility, χ'' is set zero between 25 and 30 K.*

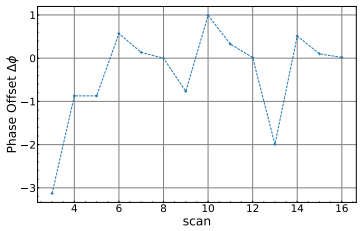

(c) *Offset distribution along a multitude of scans with different parameters. No pattern recognisable*

Fig. A.4: *AC-Mode Susceptibility Measurement, Susceptibility Phase Offset Problematic.*